Colloids and Surfaces A: Physicochemical and Engineering Aspects 692 (2024) 134037

Contents lists available at ScienceDirect

Colloids and Surfaces A: Physicochemical and Engineering Aspects

journal homepage: www.elsevier.com/locate/colsurfa

Self-shaping of triglyceride and alkane drops: Similarities and differences

Diana Cholakova *, Anita Biserova, Slavka Tcholakova, Nikolai Denkov

Department of Chemical and Pharmaceutical Engineering, Faculty of Chemistry and Pharmacy, Sofia University, 1 James Bourchier Avenue, Sofia 1164, Bulgaria

HIGHLIGHTS

- Triglycerides drops can form fluid non-spherical particles upon cooling.
- The non-spherical shape is preserved upon subsequent drop crystallization.
- Non-spherical shapes are observed only when $T_{surface\ freezing} > T_{bulk\ nucleation}$.
- When $T_{surface\ freezing} < T_{bulk\ nucleation}$ the drops freeze in spherical shape.

GRAPHICAL ABSTRACT

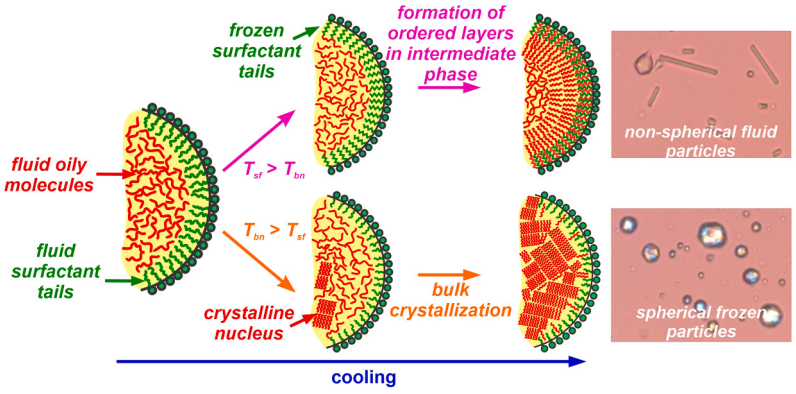

ARTICLE INFO

Keywords:
Phase transition
Triacylglycerol
Solid lipid nanoparticles
Non-spherical particles
Emulsion

ABSTRACT

Small emulsion drops typically exhibit spherical shape at positive interfacial tension due to the energy minimization principle. However, in a series of studies (Denkov et al., *Nature*, **2015**, 528, 392–395; Cholakova et al., *Nature Phys.*, **2021**, 17, 1050–1055) we showed that alkane droplets stabilized by appropriate saturated long-chain surfactants may spontaneously change their shape upon cooling, morphing into various polyhedra; hexagonal, tetragonal and triangular platelets; rod-like particles and even synthetic swimmers. These deformations are governed by the formation of thin plastic rotator phases adjacent to the drop surface. Although alkanes have numerous industrial applications, they cannot be used in food and pharma related products, in which most often triglyceride molecules are employed. The possibility for self-shaping of triglyceride drops has been demonstrated, but the detailed understanding of the process is currently missing. In the present study, we performed model experiments aimed to reveal the conditions under which the triglyceride emulsion drops may change their shape upon cooling. We show that most of the various non-spherical shapes known for alkanes can be reproduced with triglyceride droplets providing that the surfactant adsorption layer freezes before the nucleation of the oily molecules inside the drops. By comparing the behavior of triglyceride and alkane droplets, we draw unified picture and provide guiding principles which can be used for selection of appropriate surfactants enabling the spontaneous shape deformations upon cooling of oily drops of different chemical compositions.

* Correspondence to: Department of Chemical and Pharmaceutical Engineering, Sofia University, 1 James Bourchier Ave., Sofia 1164, Bulgaria.
E-mail address: dc@lcpe.uni-sofia.bg (D. Cholakova).

https://doi.org/10.1016/j.colsurfa.2024.134037
Received 5 January 2024; Received in revised form 19 April 2024; Accepted 20 April 2024
Available online 21 April 2024

1. Introduction

Micrometer sized emulsion droplets typically have spherical shape at positive interfacial tension governed by the energy minimization principle. However, in a series of studies [1–8], we showed that alkane droplets stabilized by surfactants having hydrophobic tail with length longer or up to 3 C-atoms shorter than the alkane chain can spontaneously change their shape upon cooling. The spherical drops were observed to evolve into various regular polyhedra, hexagonal, tetragonal and triangular platelets, long rod-like particles, and even thin fibers, see Fig. 1 [1–4]. Depending on the alkane-surfactant combination, even synthetic swimmers able to self-propel inside the surfactant solution, were obtained [5].

The described drop self-shaping phenomenon was found to be governed by the formation of multilayers of plastic rotator phases situated next to the drop surface, see Fig. 1e [7,8]. Rotator phases known for long-chain alkane molecules are intermediate phases between the isotropic liquid phase and the completely ordered crystalline phases in which the molecules arrange in layered structure, but the position of the individual molecules within the layers are not fully fixed, *i.e.* there is no long-range arrangement with respect to the molecule rotational degree of freedom [9,10]. The enthalpy gain due to the arrangement of a fraction of the alkane molecules into these rotator phases compensates for the increased interfacial area when non-spherical drops are formed, making them thermodynamically favored when compared to the spherical shape. Furthermore, the plastic rotator phase layers formed on the surface of the deformed drop possess the mechanical strength needed to counteract the inner capillary pressure of the liquid oil contained inside the drop, thus allowing the formation of various non-spherical shapes, including the non-trivial fluid donut shaped droplets (flattened drop with a hole in the central part), see Fig. 1b.

Another mechanism yielding to similar shape shifting upon cooling was proposed by Sloutskin and co-authors [11–13]. In their original study [11], the authors proposed that the increased surface area upon shape deformation is compensated by an ultra-low and even "transiently negative" interfacial tension which appears after the surfactant adsorption layer freezes. The energetic compensation for drop shape deformations was attributed to the relief of the elastic stress, associated with the topological defects within the curved interfacial crystal [11–13]. However, long chain length cationic surfactant was used in most of these studies and the investigated temperatures were lower than the surfactants' Krafft point. Furthermore, punctured (donut-shaped) drops were not observed by these authors.

Preparation of dispersions containing colloidal non-spherical particles may be beneficial in numerous applications. For example, non-spherical particles may be used as rheology modifiers. It has been well established, that dispersions with significantly increased viscosities can be prepared with anisotropic particles at significantly lower oil concentrations compared to those needed to obtain similar rheological properties with spherical particles [14–18]. Furthermore, the specific shape of the particles has been shown to be important for targeted drug delivery in specific organs [19–22] and for the interaction of particles with cellular membranes [23,24].

The spontaneous drop self-shaping process has been widely studied for drops composed of alkanes or mixtures of alkanes [1–8]. Although alkanes have numerous industrial applications (for example as phase change materials for energy storage [14,25–27], as lubricants in industry and cosmetics [28–31], *etc.*), their usage is limited or even prohibited in food and pharma-related products where triglycerides (TAGs) are mainly employed as hydrophobic phase. However, the self-shaping process in TAGs remains almost unexplored.

The possibility for spontaneous shape deformations of triglyceride emulsion droplets upon cooling was demonstrated initially in Ref. [2], where we showed that hexagonal trimyristin platelet particles formed upon cooling in 1.5 wt% Tween 60 surfactant solution. The self-shaping process, however, has not been investigated further and the control parameters have not been clarified.

More recently, Reiner and co-authors [32] performed investigation with cocoa butter, anhydrous milk fat, trilaurin and model binary mixtures of trilaurin (LLL), trimyristin (MMM), tripalmitin (PPP), tristearin (SSS) and triolein (OOO). These authors observed the formation of some hexagonal non-spherical shapes with cocoa butter droplets, but most of the anhydrous milk fat droplets crystallized in spherical shapes. Spherical morphologies were also observed in most of the studied binary TAG mixtures. Some fiber-like structures were observed for LLL + SSS mixed drops dispersed in 0.5 wt% Tween 20 surfactant solution. Such fibers were not observed for LLL + MMM, MMM + PPP or LLL + PPP mixed droplets. Therefore, the authors concluded that the large difference in the melting temperatures of LLL and SSS should be responsible for the observed fiber growth [32]. The underlying mechanism allowing the observed fiber formation was not explored [32].

We note that the mechanism of fibers formation in Ref. [32] seems to be distinguishably different than the self-shaping mechanism explained above [1,2,7,8]. In Ref. [32], the mixed LLL + SSS particles stabilized by 0.5 wt% Tween 20 surfactant seem to (at least partially) crystallize when temperature of 38°C was reached. However, at this stage the particles remained with spherical or close to spherical shapes. The formation of fibers protruding out of the "crystalline" droplets was observed upon further cooling (see Figure A1 in Ref. [32]). In another study exploring the bulk crystallization of such triglyceride mixtures

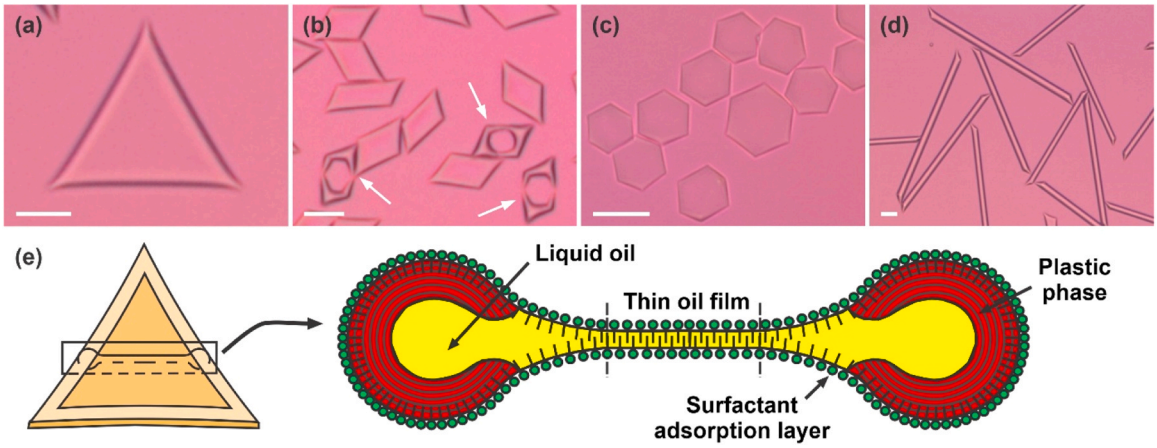

Fig. 1. (a-d) Optical microscopy images of non-spherical fluid hexadecane particles with various shapes: (a) triangular platelet; (b) tetragonal platelets part of which have a hole in their centers; (c) hexagonal platelets; (d) rod-like particles. Scale bars: 20 μm. In all experiments, the oily drops were dispersed in 1.5 wt% Tween 40 aqueous surfactant solution. (e) Schematic representation of the self-shaping mechanism. Reproduced with permission from Ref. [8]. Copyright © 2021 Elsevier Inc.

[33], we showed that a phase separation occurs in these mixtures as all TAG molecules of different length cannot arrange together in a mixed crystalline lattice even when even-numbered consecutive chain length TAGs are considered (for example LLL+MMM). When the chain length difference is larger as in Ref. [32] – the phase separation becomes even more pronounced.

Therefore, we expect that the observed fiber formation in Ref. [32] is related to the phase separation between LLL and SSS molecules occurring upon cooling. Initially, at higher temperature, the longer SSS molecules are expected to crystallize predominantly, whereas the main fraction of the shorter LLL molecules remains in a fluid state until lower temperatures are reached. Hence, the observed fibers which grow out of the already frozen particle are most probably composed of the shorter LLL molecules. Although the mechanism for fiber formation in mixed LLL+SSS drops seems to be different, the process resembles the formation of "Gorgon-like" droplets observed previously in Ref. [34]. Such structures were observed when high number of jammed latex particles were adsorbed at the alkane drop surface, thus interrupting the regular drop shape deformations upon cooling. As a result, fluid thread-like protrusions were observed to grow, originating in between the adsorbed latex particles [34].

Formation of anisotropic triglyceride particles has been also shown in the studies of Spicer and co-authors [35–37]. In these studies, comet-like crystalline particles were observed to form upon rapid cooling of oil-in-water emulsion droplets in the moment of TAG crystallization, provided that the crystal growth rate is comparable in magnitude to the dewetting rate of the still liquid fraction from the just crystallized one. This condition is met under specific requirements and was experimentally demonstrated for several triglyceride systems in the presence of sodium dodecyl sulfate (SDS) surfactant and decanol as a co-surfactant when cooling rates ≥ 5 °C/min were applied [35–37]. The elongating force in this case is the interfacial energy gradient [35].

Finally, we note that fiber-like structures were observed also upon crystallization of hydrogenated castor oil (HCO, the main triglyceride contains 12-hydroxystearic fatty acid residues) emulsion droplets stabilized by SDS, linear alkyl benzene sulfonates (with sodium, NaLAS and monoethanol amine, MEA-LAS cations) or amine oxide surfactants [38–41]. In these studies, the surfactant-to-oil ratio usually was very high, equal to or higher than 16 [16,38–41]. The mechanism in this case is argued to be related to the ability of surfactants to solubilize HCO, which then crystallizes predominantly into fiber-like structures with thickness about 10–20 nm and length between 1 and 50 μm [41]. These fibers are shown to form entangled networks which significantly modify the rheological properties of the final products, increasing their hardness and pseudoplastic behavior [16,41,42]. We note that this mechanism of fiber formation differs distinctly from the one studied in the current paper. Here, the oily emulsion drops are observed to self-shape upon cooling, without an oil solubilization being involved in the observed shape-shifting process.

Note that in numerous other studies performed with triglyceride micrometer-size emulsion droplets, no such shape deformations have been observed upon crystallization [43–48].

The aims of the present study are: 1) To perform a systematic investigation aimed to define when TAG micrometer-sized drops spontaneously change their shape before cooling and form fluid non-spherical particles of various shapes; 2) To explain the mechanism of the observed shape deformations and to define the parameters which can be used to control it; and 3) To compare the behavior of TAGs and alkanes aiming to define unified principles which should be met to observe drop shape deformations driven by surface phase transitions.

The paper is structured as follows: Section 2 presents the materials and experimental methods used; Section 3 presents the experimental results and their interpretation. It is divided into four sub-sections: The experimental results obtained with TAG drops are presented in Section 3.1. Section 3.2 discusses the structural difference between the arrangement of alkane and TAG molecules in crystalline phases. Results with alkane droplets stabilized by the same surfactant solution as those used for TAG emulsions are presented in Section 3.3. A comparison between alkanes and TAGs is presented in Section 3.4, where the mechanisms are also discussed. In the final Section 4, the most important findings are summarized.

2. Materials and methods

2.1. Materials

Trilaurin (LLL, C_{12}TAG) with purity > 98 % and tetracosane ($C_{24}H_{50}$) with purity > 99 % were mainly used as hydrophobic phases in the prepared oil-in-water emulsions. Both substances were purchased from TCI Chemicals. In part of the experiments we used tricaprin (C_{10}TAG, purity > 98 %, TCI Chemicals) and tricosane ($C_{23}H_{48}$, purity 99 %, Sigma-Aldrich).

Emulsions were stabilized by various surfactants. The nonionic water-soluble surfactants included polyoxyethylene alkyl ethers with a general formula C_nEO_m: $C_{12}EO_{23}$ (trade name Brij 35, Sigma-Aldrich), $C_{18}EO_{20}$ (Brij S20, Sigma-Aldrich) and $C_{20-40}EO_{40}$ (Performathox 480, New Phase Technology); polyxyethylene sorbitan alkyl ethers, C_nSorbEO$_{20}$: C_{12}SorbEO$_{20}$ (Tween 20, Sigma-Aldrich) and C_{16-18}SorbEO$_{20}$ (Tween 60, Sigma-Aldrich). Nonionic oil-soluble surfactants were also studied, including $C_{12}EO_4$ (Brij L4, Sigma-Aldrich), $C_{18}EO_{20}$ (Brij S2, Sigma-Aldrich), $C_{20-40}EO_3$ (Performathox 420, New Phase Technology) and monostearin (TCI Chemicals). Note that all these surfactants are of technical grade and contain mixtures of molecules, mainly with different numbers of ethoxy groups in the hydrophilic domain of the molecule [49].

The ionic stearoyllactic acid sodium salt (sodium stearoyllactate, TCI Chemicals, product code S0846) and behentrimonium chloride (C_{22}TAC) surfactants were also tested. We also used long chain fatty acids and fatty alcohols, including 1-octadecanol (C_{18}OH, Fisher Scientific), 1-docosanol (C_{22}OH, TCI Chemicals), palmitic acid (C_{16}Ac, Sigma) and behenic acid (C_{22}Ac, TCI Chemicals).

All substances were used as received. The aqueous surfactant solutions were prepared with deionized water, purified by Elix3 Module, Millipore.

2.2. Methods

2.2.1. Emulsion preparation

The studied emulsions were prepared either using rotor-stator homogenizer (Ultra Turrax T25, IKA) or by membrane emulsification technique (Shirasu Porous Glass membranes, SPG, Miyazaki, Japan) when monodisperse droplets were needed. A detailed description of the procedure used for membrane emulsification can be found in Refs. [1,2]. All samples were prepared and stored at temperature which was at least 5°C higher than the bulk melting temperature of the dispersed oil to ensure that it remains in a liquid state during storage before the subsequent cooling experiments. Unless otherwise noted explicitly, the concentration of the oil-soluble surfactant (if present) was 1 wt% with respect to the weight of the oil phase, while the concentration of the water-soluble surfactant was 1.5 wt% with respect to the weight of the aqueous phase. These concentrations were chosen to be significantly higher than the critical micellar concentrations of the respective surfactant.

2.2.2. Optical microscopy observations

The behavior of the emulsified oily droplets upon temperature variations was studied using optical microscopy observations with microscope AxioImager.M2m (Zeiss, Germany) in polarized white light with included λ-plate situated at 45° between the polarizer and analyzer. The investigated emulsion samples were placed in rectangular borosilicate glass capillaries (VitroTubes, CM Scientific) with height of 0.1 mm and width of 1 or 2 mm. The capillary with the studied sample was placed in

a specially designed aluminium thermostatic chamber with optical windows. The chamber was connected to a cryo-compact circulator (Julabo CF30) allowing precise temperature control. The exact temperature in the studied sample was monitored using calibrated thermocouple probe inserted in a neighboring orifice of the aluminum chamber. Cooling rates of ≈ 0.3–1 °C/min were used in the present study. Further details about the experimental set-up and the imaging conditions can be found in Refs. [1–8].

2.2.3. Interfacial tension measurements

The interfacial tension (IFT) measurements were performed with Spinning drop tensiometer (Krüss, Germany). In this method a drop of the lighter phase (oil) is formed in capillary filled with the denser (aqueous) phase. The capillary is set in rotation which causes the oily drop to elongate by the centrifugal forces which are balanced by the interfacial tension. The shape of the drop is monitored during the experiment and then the drop curvature is analyzed using the Young-Laplace approach. This analysis allows precise measurements of interfacial tensions ranging between 10^{-6} and *ca.* 20–30 mN/m.

In the present study, we used droplets with volume of ca. 1–10 μL. The rotation speed was chosen to be high enough to deform the droplet from its spherical shape. The measurements were performed upon cooling from high temperature until the drop begins to freeze. The applied cooling rate was ≈ 0.6 °C/min to mimic the one used in the optical microscopy experiments. At least three independent experiments were performed for each system and the results presented within the manuscript are averaged between them.

For precise determination of the IFT, the density of the studied liquids as a function of temperature should be known. The density of tetracosane at different temperatures was determined using the relation $\rho_{C24}(T) = (1.224 + 1.114 \times 10^{-3}T)^{-1}$, where T is the temperature in degrees Celsius [50]. For LLL, we used linear interpolation between two experimental values available in the literature: $\rho_{\mathrm{LLL}} \approx 0.8801$ g/ml at 80°C [51] and $\rho_{\mathrm{LLL}} \approx 0.9085$ g/ml at 40°C [52]. Hence, the density of the trilaurin was determined as: $\rho_{LLL}(T) = 0.937 - 7.1 \times 10^{-4}T$, where T is in degrees Celsius.

DSC

The differential scanning calorimetry (DSC) measurements were performed with Discovery DSC 250 (TA Instuments, USA). A detailed description of the experimental procedure can be found in Ref. [7]. The studied bulk oils were first melted at temperature at least 10°C higher than their melting temperature and kept at this temperature for at least 10 min. Then the samples were cooled and heated at 1 °C/min rate three consecutive times. At least two independently prepared samples were tested. All obtained results were with excellent reproducibility.

3. Results and discussion

3.1. Spontaneous deformations of TAG droplets

This section presents the results from the systematic study aiming to understand which are the appropriate surfactants able to induce spontaneous shape deformations in TAG emulsion drops upon cooling.

In the studies performed previously with alkane droplets, we showed that the self-shaping process is typically observed when a surfactant with hydrophobic tail longer, equal or up to 3 C-atoms shorter than the alkane chain length is used. In the present study, we used mainly LLL droplets as this triglyceride has the most convenient melting temperature, $T_m \approx 46$°C [53].

Trilaurin molecules (LLL or C_{12}TAG) contain three lauric acid (C_{12}Ac) residues connected by ester bonds to a glycerol backbone. Therefore, we began our experiments by preparing LLL emulsions stabilized by three different nonionic surfactants containing C_{12} alkyl chains: the oil-soluble Brij L4 ($C_{12}EO_4$) and the water-soluble – Brij 35 ($C_{12}EO_{23}$) and Tween 20 (C_{12}SorbEO$_{20}$). Illustrative pictures showing frozen LLL particles obtained in these experiments are shown in Fig. 2a, b. As seen from the pictures, these LLL droplets did not evolve in shape upon cooling and froze in the typical spherical shape without any observable shape changes. The freezing process was observed after significant subcooling. The first freezing events started in bigger droplets ($d_{ini} > 10$ μm) at *ca.* 13°C for Brij L4 stabilized emulsion and at lower temperature of ≈ 7°C for Tween 20 stabilized sample. The smaller drops froze at even lower temperatures approaching 0°C. Although these temperatures are relatively low, they are probably not sufficient to induce freezing in the surfactant adsorption layer of C_{12}-tail surfactants. Note that the melting point of *n*-dodecane ($C_{12}H_{26}$) is $T_m \approx -10$°C [10]. Therefore, next we studied longer-chain surfactants.

Fig. 2c-f presents a collection of non-spherical fluid LLL particles obtained upon cooling of (initially) spherical LLL droplets, dispersed in various solutions containing stearoyl chain (C_{18}) surfactants. As seen from these pictures, the formation of non-spherical fluid particles is possible when triglyceride droplets are used. In these particular experiments, sodium stearoyllactate (Fig. 2c) or Brij S20 ($C_{18}EO_{20}$, Fig. 2d-f) were used. In the sample stabilized by sodium stearoyllactate surfactant, we observed the formation of punctured donut-like particles which remained stable for a long period of time (several minutes) before the freezing temperature of the drops was reached, Fig. 2c. In this particular system, the first drop shape deformations were observed at *ca.* 30°C, while the main fraction of the drops began to freeze at ≈ 9°C. We note

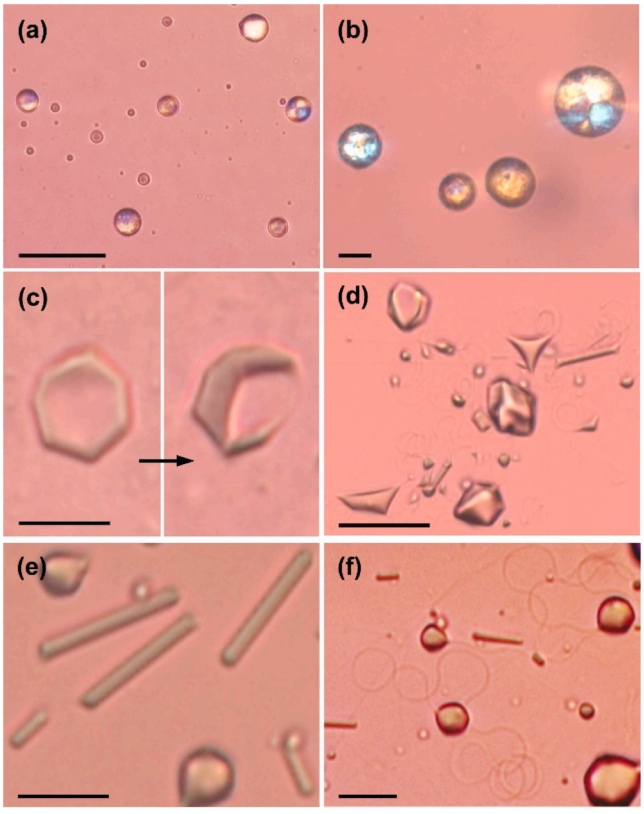

Fig. 2. Self-shaping of LLL droplets dispersed in various surfactant solutions. (a,b) Spherical frozen particles obtained upon cooling of LLL emulsion droplets stabilized by: (a) Tween 20 or (b) Brij L4 surfactants. **(c)** Hexagonal platelet particle which punctures in its center, while the main part of the oil remains in fluid state. Sodium stearoyl lactate was used as surfactant in this experiment, $T_d \approx 32$°C. **(d)** Collection of non-spherical particles with different shapes obtained upon cooling of LLL drops stabilized by Brij S20 surfactant, see also Supplementary Movie 1 where the complete transformation sequence for this particular sample is presented. **(e,f)** Rod-like fluid particles along with non-spherical droplets extruding long thin fibers. Brij S20 and dodecanol were used in the preparation of this emulsion, $T_d \approx 16$°C. Cooling rate ≈ 1 °C/min was used in all experiments. Scale bars: 10 μm.

that the platelet puncturing is related to the thinning of the central part of the platelet and instability of the thin water-oil-water film formed therein, as previously shown by reflected light experiments in Refs. [54,55].

Supplementary material related to this article can be found online at doi:10.1016/j.colsurfa.2024.134037.

Formation of various non-spherical particles was observed also for Brij 20 stabilized emulsions, see Fig. 2d and Supplementary Movie 1. In this system, along with the spontaneous drop deformations, multiple drop breakage events occurred upon cooling, resulting in the formation of higher in number and smaller in size emulsion droplets (as compared to the initial emulsion). We note that this breakage phenomenon, caused by the breakage of the ordered phase situated on the drop surface, was previously observed with alkane droplets stabilized by this and other surfactants. A detailed description of this self-emulsification process, along with results showing its efficiency, is available in Refs. [54,55].

These results evidence that fluid non-spherical LLL particles can be prepared when C_{18} surfactants are used for emulsion stabilization, whereas the LLL drops freeze in spherical shape in presence of the shorter chain C_{12} surfactants. Non-spherical shapes of LLL drops were obtained also with other long-chain surfactants, including monostearin, behenyl trimethyl ammonium chloride, Tween 60, and some long-chain alcohols and acids (octadecanol, hexadecenoic acid, behenic acid), see Supplementary Figure S1. Similar non-spherical particles were also obtained in experiments with tricaprin droplets with pre-dissolved octadecanol in them, dispersed in Brij S20 surfactant solution. Thus, we have confirmed that non-spherical self-shaping TAG drops are formed in the presence of various long-chain surfactants.

Next, we discuss the difference in the arrangement of alkane and triglyceride molecules in their crystalline phases, which is of crucial importance to understand the reasons for the observed differences (e.g. the chain length difference, Δn, between the surfactant and oil chains at which deformations are observed) and the related self-shaping mechanism.

3.2. Alkanes vs triglycerides: comparison of ordered structures

C_{12}TAG (LLL) has melting temperature of $T_m \approx 46°C$, whereas the alkane with 12 C-atoms in its chain (dodecane, $C_{12}H_{26}$) melts at $T_m \approx -10°C$ [10]. This significant difference is governed by the fact that the triglyceride molecules contain not a single, but three individual C_{12} chains connected to a glycerol backbone. The glycerol backbone, however, contains oxygen atoms which make this part of the molecule more polar. Therefore, in crystalline state the monoacid saturated TAG molecules usually arrange in double chain-length structure (2 L), where two of the alkyl chains point in the same direction, whereas the third chain is oriented in the opposite direction, see Fig. 3 [53]. In this way, the oxygen atoms minimize their unfavorable contact with the hydrocarbon chains. This 2 L arrangement determines the significantly higher melting point for C_{12}TAG as compared to $C_{12}H_{26}$ alkane. Hence, the comparison between LLL and alkanes should not be made with dodecane, but rather with tetracosane ($C_{24}H_{50}$, denoted as C_{24}) which contains two times longer hydrocarbon chain. Indeed, the tetracosane has a melting temperature $T_m \approx 51°C$ [10], which is closer to the melting temperature of LLL.

Another distinction between the alkanes and triglycerides is the formation of intermediate phases upon cooling from a molten state. The long-chain alkanes arrange in intermediate in structure rotator phases (denoted as R_I to R_V), while the triglycerides are known to form three different crystalline polymorphs: α, β' and β [10,53,56]. The molecules in R phase are known to have limited rotational freedom and may oscillate around their long axis. The TAG's polymorphs are usually considered as crystalline states. However, as initially suggested by Small [57], the least stable α polymorph has similarities to the rotator phases in alkanes, as the acyl chains in α polymorph and particularly the C-atoms positioned close to the chain-ends possess significant molecular freedom and are able to perform torsional oscillations [58–60].

Noting this significant difference in the molecular arrangement of TAGs and alkanes, next we studied the self-shaping process of emulsion droplets composed of long chain alkanes (tetracosane and tricosane) to check whether their behavior is similar to that observed with triglyceride drops.

3.3. Spontaneous drop deformations in long chain alkanes

To test whether the surfactants able to induce spontaneous shape changes in LLL drops are also able to induce deformations in alkane drops, experiments with tetracosane (C_{24}) emulsion droplets containing pre-dissolved oil-soluble surfactants and dispersed in aqueous solution of Brij S20 were performed. Drop shape deformations were not observed in any of the studied systems containing tetracosane droplets and surfactants with hydrophobic tails of $\leq$ 18 C-atoms, see Supplementary Figure S2, although these same surfactants were able to induce deformations in LLL drops. The freezing of tetracosane droplets occurred at relatively small subcooling of 2–3°C only. Note that these C_{18}-tail surfactants do not meet the requirement formulated by our previous investigations of alkane droplets with $C_n \leq 20$ stating that the chain length difference between the surfactant hydrophobic tail and the alkane chain length should be $\Delta n \leq 3$ C-atoms to allow formation of non-spherical fluid particles upon cooling [1,2].

For this reason, next we studied tetracosane droplets stabilized by longer chain surfactants. As seen from the pictures shown in Fig. 4, drop shape deformation do occur with these droplets. The deformations of C_{24} droplets with $d_{ini} \gtrsim 5$ μm began at temperatures close to the bulk melting temperature of C_{24} ($T_m \approx 51°C$) and proceeded very quickly before the drops crystallize at a few degrees' lower temperatures. Formation of rotator phase occupying the whole drop volume prior to the formation of the crystalline phase was also observed in some fraction of the droplets. This process is illustrated with the two images shown in the bottom row in Fig. 4c and in Supplementary Figure S3. The faint colors seen

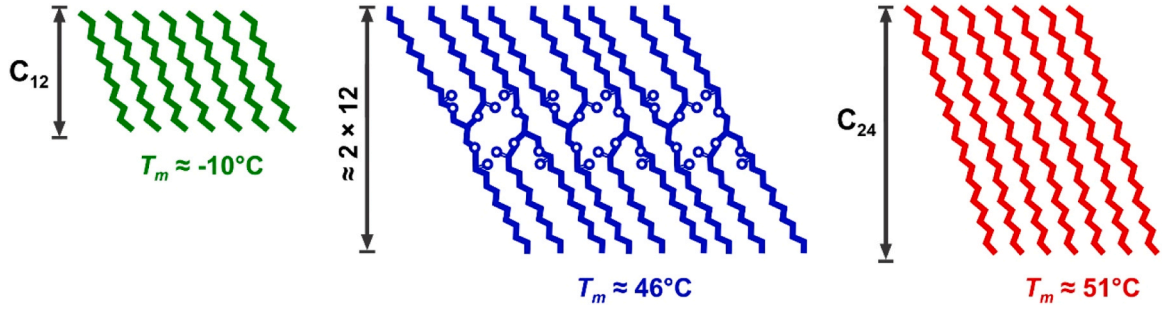

Fig. 3. Schematic presentation of the alkane (green, red) and TAG (blue) molecules arrangement in a crystalline triclinic phase. The monoacid TAG molecules (C_nTAG) usually arrange in 2 L chain-length structure, which determines that their melting point is much closer to alkane with $2n$ C-atoms in the chain compared to alkanes with n C-atoms. An example for $n = 12$ is presented in the figure.

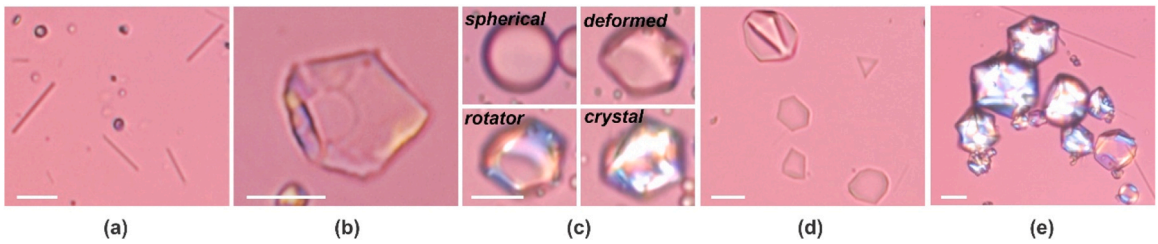

Fig. 4. Optical microscopy pictures of non-spherical alkane particles. (a-c) C_{24} alkane; (d,e) C_{23} alkane. The samples are stabilized by: (a,b,d) C_{22}TAC; (c,e) C_{22}OH + Performathox 480. (a) Fluid rod-like particles; (b) Frozen platelet; (c) Formation of crystalline polyhedron. First, drop shape deformations are observed at $T_d \approx 49°C$, formation of plastic rotator phase occupying the whole particle volume is observed at $T \approx 48.2°C$. The rotator phase transforms into crystalline phase upon further cooling to $T \approx 47.2°C$. (d) Fluid non-spherical particles of various shapes; (e) Frozen polyhedra. Scale bars: 10 μm.

predominantly in the particle periphery in the left-hand image indicate the formation of a rotator phase occupying the entire drop volume, which occurs at $T \approx 48.2°C$. This bulk rotator phase remains present for ca. 1 min before the final crystallization takes place via a rotator-to-crystal phase transition at $T \approx 47.2°C$, see the right-hand image in the bottom row in Fig. 4c. Following this transition, the colors become significantly more intensive and occupy the entire particle volume. No further changes occur even with further temperature decrease, see Supplementary Figure S3. We note that these observations closely resemble those made with hexadecane drops in Ref. [8], see e.g. Figures 7c, 9 or Supplementary Figures S6, S7 and S8 in Ref. [8]. In this previous study [8], we showed unambiguously, using X-ray scattering and optical microscopy experiments, that drops structured in rotator phase have lower melting temperature compared to the fully crystalline drops and that the rotator-to-crystal phase transition is accompanied with similar color changes as those observed in Fig. 4c.

The shape deformations in smaller C_{24} drops began at slightly lower temperatures ($T \approx 43 \pm 2$ °C) and the drops froze when the temperature was decreased to *ca.* 37°C. Note that all these temperatures are higher compared to the temperatures at which the drop deformations started with the LLL drops ($T_d \approx 10–35°C$, depending on the specific surfactant) and the temperatures at which the LLL drops froze (usually $T_f \approx 0–20°C$, depending on the surfactant/drop size).

Experiments were also performed with C_{23} alkane (tricosane) which has melting temperature $T_m \approx 49°C$. As expected, the surfactants which were able to induce drop shape deformations with the longer C_{24} alkane, also induced drop shape transformation with the shorter C_{23} alkane, see Fig. 4d,e.

These results demonstrate that although for alkanes the chain length difference between the alkane chain and surfactant tail (Δn) can be used to predict whether drop shape deformations will be observed upon cooling of a given system, this rule is not universal for different oils. Therefore, another more universal rule should be formulated to include all possible scenarios. This is done in the next section where we discuss also the mechanism of drop shape deformations in TAG drops.

3.4. Drop shape deformations in alkane and TAG drops – a comparison

As explained in the Introduction section – two different mechanisms have been proposed to explain the formation of fluid non-spherical particles upon cooling. In most of the systems, studied by Denkov and co-authors [1–8], the rotator phase mechanism was shown to be operative where the increase of the surface area proceeds at positive interfacial tension. The related surface energy increase is compensated by the formation of thin layers (thickness between *ca.* 5 and 100 nm has been estimated [7]) of plastic rotator phases situated next to the drop surface. In the systems, studied by Sloutskin et al. [11–13], another mechanism was found to be operative, where the increase of the surface area proceeds at ultra-low interfacial tension after the freezing of the surfactant adsorption layer. Thus, the surface area increase does not lead to energetic penalty.

To check which of these two mechanisms is operative in the systems investigated in the present study, we performed interfacial tension measurement with some of the studied systems. Spinning drop method was used for these experiments because it allows precise measurements of low interfacial tensions, even below 0.1 mN/m [61,62]. In this method, an oily drop with average volume between 1 and 10 μl (diameter ≈ 0.6–1.3 mm) is placed in rotating thin capillary. The liquid droplet elongates under the action of the centrifugal forces, until they become balanced by the interfacial tension [63].

Fig. 5a presents the experimental results obtained with C_{24} and LLL droplets in presence and in absence of oil-soluble surfactant Brij S2. In both cases, the oily drops are immersed in Brij S20 surfactant solution. Drop shape deformations starting around 20°C were observed in the experiments with micrometer-sized drops for LLL + Brij S2 in Brij S20 system, whereas the freezing started at $T \approx 12°C$, see Fig. 2d and Supplementary Figure S1. In contrast, no deformations are observed in C_{24} ± Brij S2 in Brij S20 emulsions, see Supplementary Figure S2.

The interfacial tensions measured in the presence of both oil- and water-soluble surfactants were lower than those measured in the presence of water-soluble surfactant only, compare the full and empty symbols of same type in Fig. 5a. However, although the LLL drops undergo shape deformations upon cooling and the C_{24} drops do not, the IFTs measured with LLL system were higher than those measured with C_{24}. In agreement with the observations performed with micrometer-size droplets, the LLL drops used for IFT measurements froze at significantly lower temperatures compared to C_{24} drops, see the black points in Fig. 5 which show the last experimental value which can be obtained before the crystallization of the studied oily drop begins. Interfacial tension measurements were also performed with LLL drop immersed in a solution containing 0.3 wt% sodium stearoyllactylate. This particular system was chosen because deformations in micrometer-sized droplets began at significantly higher temperatures compared to those in Brij systems, $T_d \approx 35 \pm 1°C$. Therefore, this system allowed determination of the IFT values at temperatures higher and up to 7°C lower than T_d observed from the microscopy experiments, before the (millimeter-sized) drop used for IFT measurements began to freeze at around 28°C. These measurements show significantly higher IFT values, $\sigma \approx 27$ mN/m at $T \approx 35°C$ and $\sigma \approx 25.5$ mN/m at $T \approx 28°C$. Note that pendant drop method was used for these measurements due to the high IFT values, see Ref. [6] for explanation of the exact experimental procedure.

Similar results, showing high interfacial tension at temperatures, at which the drop shape deformations are observed in the emulsion drops, were obtained with C_{24} drops containing pre-dissolved 1 wt% C_{22}OH and immersed in 1.5 wt% Performatox 480 solution, see Supplementary Figures S3 and S4. For this particular system, the drop shape deformations began at $T \approx 49°C$ (see Fig. 4c and Supplementary Figure S3). At this temperature, the measured IFT was 7.2 ± 1 mN/m, see Supplementary Figure S4.

The IFT results show unambiguously that the observed shape deformations can occur without having ultra-low interfacial tension. Therefore, the mechanism including the formation of intermediate

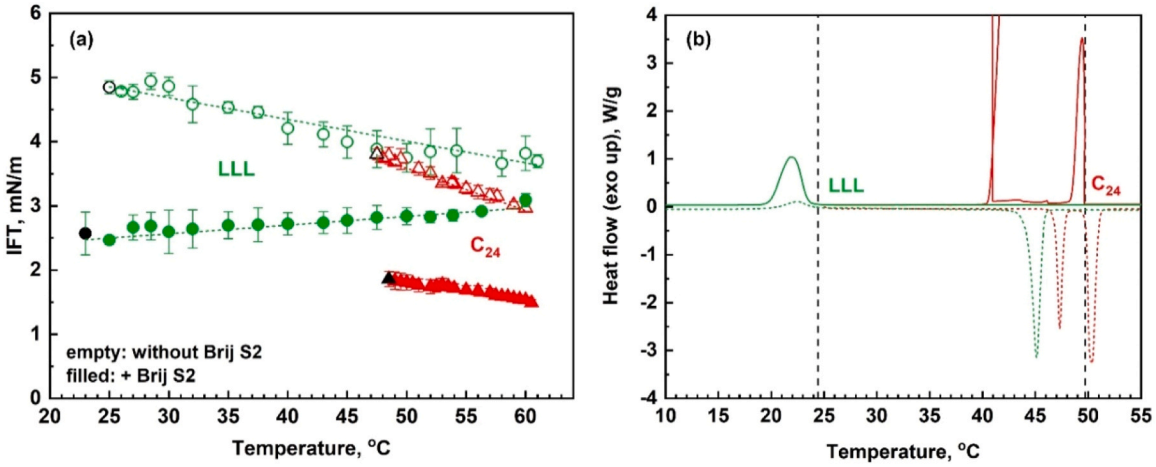

Fig. 5. IFT and DSC data. (a) Interfacial tension dependence from temperature for LLL (green symbols) and C_{24} (red symbols) drops immersed in Brij S20 surfactant solution. The experiments are performed with (full symbols) or without (empty symbols) pre-dissolved Brij S2 in the oily phase. The black symbols show the last values which can be measured before the oily drop begins to freeze. (b) DSC data for bulk LLL and C_{24} sample. The vertical dashed lines denote the temperatures at which the formation of *R* phase (for C_{24}) or α-polymorph (for LLL) starts. Note that these temperatures differ by ca. 25°C, although the melting temperatures of these substances differ by only 5°C.

plastic phases, situated next to the drop surface after the surfactant adsorption layer freezes, should be operative in this case. Note that, there could be other triglyceride-surfactant combinations in which the mechanism proposed by Sloutskin's et al. might be operative [11–13]. Furthermore, assuming that the rotator phase mechanism underlies the presently observed phenomenon, one could easily explain also all the different experimental observations made with TAG drops: Drop shape deformations can be observed with TAG drops because TAGs can form three different polymorphic forms upon cooling from melt. The least stable, α polymorph, is similar to *R* phases of alkanes. Drop shape deformations are not observed with LLL (C_{12}TAG) drops stabilized by C_{12}-tail surfactants as these surfactants are unable to freeze on the drop surface before a crystalline nucleus appear in the drop volume. For that reason, longer chain surfactants are needed.

The obtained results show also that the chain-length difference between the monoacid TAG with hydrocarbon chains of length C_y and surfactant with saturated hydrophobic tail C_x should be defined as $\Delta n = 2y - x$, because TAG molecules arrange in 2 L structure. For alkane with length *z* and surfactant with tail C_x, a chain length difference $\Delta n = z - x \leq 3$ is needed to observe shape shifting upon cooling. This chain length difference can be higher for TAG drops. For example – we have observed shape deformations in systems for which $\Delta n = 6$, see Fig. 2.

This apparent contradiction between Δn at which drop deformations are observed in TAG and alkane emulsions is explained with the significantly hindered nucleation in TAG systems, compared to alkanes, due to their significantly higher molecular mass. According to the classical nucleation theory, the rate of homogeneous nucleation (v) per unit volume can be expressed as:

$$v = \rho Z j \exp\left(-\frac{\Delta G^*}{k_B T}\right),$$

where ρ is the number density of molecules, j is the rate at which the molecules attach to the nucleus and cause its growth, Z is the Zeldovich factor, ΔG^* is the free energy cost for creation of a critical nucleus, k_B is the Boltzmann constant, and T is the temperature [64,65]. An upper bound for the value of j can be acquired if a diffusion-limited flux of molecules onto the growing nucleus is assumed, $j \simeq \rho D R^*$, where D is the diffusion coefficient for the molecules and R^* is the radius of critical nucleus [65]. Numerous investigations have shown that there is a non-linear dependence between the diffusion coefficient and molecular mass, $D(M_w,T) = AM_w^{k(T)}$, where A is constant and $k(T) \approx -2$ at elevated temperatures [50]. The molecular weight of LLL is M_w (LLL) = 639.02 g/mol, while for C_{24} it is about 50 % lower, M_w ($C_{24}H_{50}$) = 338.65 g/mol. Accordingly, the diffusion coefficient of alkane molecules is about two orders of magnitude higher compared to those for LLL: D (C_{24}) $\approx 1.8 \times 10^{-10}$ m^2/s at 30°C and D (C_{24}) $\approx 2.8 \times 10^{-10}$ m^2/s at 50°C [50], whereas values of the order of 10^{-12} m^2/s were reported for TAGs [66,67]. Note that ΔG^* is expected also to be higher for triglycerides in comparison to alkanes, thus leading to a reduced nucleation rate in triglyceride systems. This is attributed to the intricate molecular structure of TAG molecules compared to alkanes, which limits the number of appropriate molecular conformations which should be adopted by the neighboring TAG molecules to allow formation of stable crystalline nucleus.

The hindered nucleation in TAG systems is directly evidenced by the significantly decreased temperature at which the TAG drops crystallize compared to C_{24} drops, although both bulk materials have comparable melting temperatures. Furthermore, similar result is obtained if the crystallization in bulk oils is compared – while the formation of rotator phase in C_{24} bulk sample begins at *ca.* 50°C upon 1 °C/min cooling from melt, the formation of α polymorph in LLL sample starts at *ca.* 25°C under equivalent experimental conditions, see the DSC thermograms presented in Fig. 5b.

These observations allowed us to revise and specify the initially proposed condition for appearance of drop shape deformations to capture the results obtained with TAG drops as well. The schematic representation of the mechanism is shown in Fig. 6. Two opposing processes are possible upon cooling of emulsion droplets: (1) A bulk nucleus of critical size may appear in the drop volume and then grow, which results in the formation of spherical frozen particle, see the lower branch in Fig. 6; or (2) The surfactant adsorption layer may freeze before the bulk nucleus appears and act as a template. Then the oily molecules situated next to the drop surface arrange in multilayers of intermediate phase, thus allowing the formation of fluid non-spherical drops with various shapes, see the upper branch in Fig. 6. Depending on which of these two processes occurs first (*i.e.* at higher temperature) – drop shape deformations are or not observed in oil-in-water emulsions at positive interfacial tension.

This mechanism also explains why deformations in smaller droplets are generally easier and more pronounced compared to those in larger drops within systems of equivalent chemical compositions. The volume of a droplet (V) is proportional to the cube of its radius (R), $V = (4\pi R^3)/3$. Consequently, reducing the droplet size results in a substantial decrease in volume, thereby decreasing the probability of stable nucleus

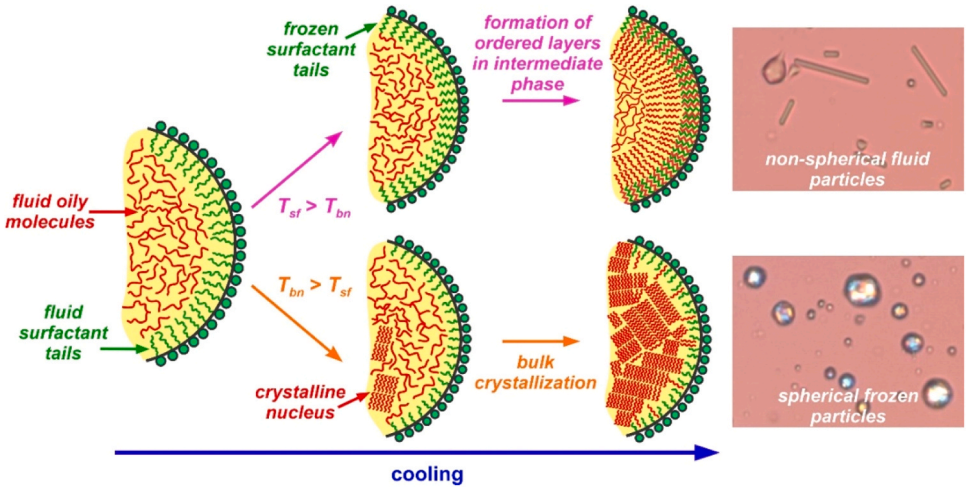

Fig. 6. Schematic presentation of the processes occurring upon cooling of oily droplets. At high temperatures both the surfactant adsorption layer and oily molecules in the drop volume are in a fluid state. The formation of non-spherical fluid shapes upon cooling depends on the comparison between the surface freezing temperature (T_{sf}) and the temperature at which a stable nucleus would form inside the drop volume (T_{bn}). When $T_{sf} > T_{bn}$ the freezing of the surfactant adsorption layer induces the formation of ordered layers of oily molecules next to the drop surface which enable the formation of non-spherical fluid particles. In the opposite case, $T_{sf} < T_{bn}$, the bulk nucleation occurs first, leading to the formation of spherical frozen particles.

formation and crystallization of the entire droplet volume. Thus, under equivalent experimental conditions, smaller drops would have a longer time available for the self-shaping process before bulk nucleation takes place. Note that bulk nucleation occurs within the timeframe of our experiments, as illustrated in Fig. 2a,b and Supplementary Figure S2 – the drops freeze into a spheroidal shape after the formation of a bulk nucleus.

The temperature at which the crystallization begins for bulk oil can be used as an estimate for T_{bn}, whereas the surface freezing temperature T_{sf} can be estimated from the literature data about the bulk melting point of the alkane with length equivalent to that of the hydrophobic tail of the surfactant. For example, the formation of α polymorph for LLL upon cooling begins at *ca.* 25°C. Deformations in these drops are observed with C_{18}-tail surfactants. The equivalent alkane, octadecane, has melting temperature $T_m \approx 29°C > 25°C$. Therefore, one could expect that C_{18}-surfactants are able to induce drop shape deformations upon cooling, just as observed experimentally.

Note that this study exclusively considers oils of high purity. If we aim to apply the conclusions drawn from this study to more intricate systems that encompass mixtures of molecules or natural triglyceride oils (where the majority of TAG molecules possess fatty acid residues of different lengths), then the chemical component that crystallizes at the highest temperature should be identified. Its crystallization temperature should then be compared to the temperature for the surface freezing of the surfactant. Furthermore, in these intricate systems, additional challenges may emerge in achieving a suitable arrangement of different molecules due to their incompatible structures. Therefore, although we anticipate the feasibility of the self-shaping process in such systems, a more comprehensive and detailed study is required to check if additional requirements exist. This investigation goes beyond the scope of the present study.

4. Conclusions

In the present study, the possibility for formation of non-spherical fluid TAG particles from initially spherical emulsion droplets upon cooling was investigated. We showed that such deformations, previously observed with alkane systems [1–8], are possible also for TAG droplets at positive interfacial tensions, providing that a suitable TAG/surfactant combination is chosen. This was explained with the fact that TAGs can form intermediate in stability phase (α polymorph) prior to the formation of the most ordered β polymorph.

The comparison between the behavior of TAG and alkane drops allowed us to propose a unified condition which should be met to allow the formation of non-spherical fluid droplets upon cooling. In addition to the ability of the oily molecules to form intermediate in structure phase between the fully isotropic liquid phase and the completely ordered crystalline phase, a comparison between the temperatures for bulk oil nucleation (T_{bn}) and for surface freezing of the surfactant adsorption layer (T_{sf}) should be made. When $T_{bn} > T_{sf}$, the emulsion droplets freeze in spherical shape without any significant change in their shape. In the opposite case, $T_{bn} < T_{sf}$, the surfactant adsorption layer freezes prior to the formation of bulk nucleus and then it serves as a template for formation of ordered layers of oily molecules next to the drop surface. In this case, drop shape deformations upon cooling are observed. An estimate for T_{bn} can be made by determining the onset temperature for bulk crystallization of the oily phase of interest in DSC measurements (under similar cooling protocol). Note that T_{bn} depends strongly on the molecular arrangement obtained upon cooling and may be significantly different than T_m for the respective oil. T_{sf} can be estimated from the bulk melting temperature of alkane with chain length equal to the length of the saturated hydrophobic tail of the studied surfactant.

The present study complements the previously described principles governing the unusual phenomenon of spontaneous drop self-shaping upon cooling. The precise formulation of the underlying principles for formation of non-spherical particles with triglycerides significantly enlarge its area of application, allowing it to be used for various systems of industrial importance *incl.* cosmetics, foods, beverages, and pharmaceutics. While the experiments in this study were exclusively conducted with TAGs of high purity, we anticipate that similar results can be obtained also with natural TAG oils (such as coconut oil, palm kernel oil, cocoa butter, and others), provided that surfactants satisfying the defined principles are used for the stabilization of the prepared emulsions.

CRediT authorship contribution statement

Nikolai Denkov: Writing – review & editing, Supervision, Funding acquisition, Conceptualization. **Slavka Tcholakova:** Writing – review & editing, Supervision, Conceptualization. **Anita Biserova:** Visualization, Investigation. **Diana Cholakova:** Writing – review & editing, Writing – original draft, Visualization, Validation, Methodology, Investigation, Formal analysis, Conceptualization.

Declaration of Competing Interest

The authors declare that they have no known competing financial interests or personal relationships that could have appeared to influence the work reported in this paper.

Data availability

Data will be made available on request.

Acknowledgements

The study was funded by Bulgarian Ministry of Education and Science, under the National Research Program "VIHREN", project ROTA-Active (no. KP-06-DV-4/16.12.2019). The authors acknowledge the possibility to use Spinning drop tensiometer, purchased for execution of project BG05M2OP001–1.001-0008, Operational Program "Science and Education for Smart Growth", Bulgaria. The authors are grateful to Mr. M. Pantov (Sofia University) for performing a small fraction of the optical microscopy experiments and for measuring the interfacial tensions.

Part of this work was performed in preparation for execution of proposal "Active Micro-droplets under Microgravity Conditions" (ESA-DLR-FLUMIAS-2020–022) selected to be executed from the DLR/ESA FLUMIAS-ISS 2020 AO call.

Appendix A. Supporting information

Supplementary data associated with this article can be found in the online version at doi:10.1016/j.colsurfa.2024.134037.

References

[1] N. Denkov, S. Tcholakova, I. Lesov, D. Cholakova, S.K. Smoukov, Self-shaping of oil droplets via the formation of intermediate rotator phases upon cooling, Nature 528 (2015) 392–395, https://doi.org/10.1038/nature16189.
[2] D. Cholakova, N. Denkov, S. Tcholakova, I. Lesov, S.K. Smoukov, Control of drop shape transformations in cooled emulsions, Adv. Colloid Interface Sci. 235 (2016) 90–107, https://doi.org/10.1016/j.cis.2016.06.002.
[3] D. Cholakova, Z. Valkova, S. Tcholakova, N. Denkov, S.K. Smoukov, Self-shaping" of multicomponent drop, Langmuir 33 (2017) 5696–5706, https://doi.org/10.1021/acs.langmuir.7b01153.
[4] D. Glushkova, D. Cholakova, A. Biserova, K. Tsvetkova, S. Tcholakova, N. Denkov, Drop shape stability vs shape shifting: role of surfactant adsorption layer, Colloids Surf. A 656 (2023) 130374, https://doi.org/10.1016/j.colsurfa.2022.130374.
[5] D. Cholakova, M. Lisicki, S.K. Smoukov, S. Tcholakova, E.E. Lin, J. Chen, N. Denkov, Rechargeable self-assembled droplet microswimmers driven by surface phase transitions, Nat. Phys. 17 (2021) 1050–1055, https://doi.org/10.1038/s41567-021-01291-3.
[6] N. Denkov, D. Cholakova, S. Tcholakova, S.K. Smoukov, On the mechanism of drop self-shaping in cooled emulsions, Langmuir 32 (2016) 7985–7991, https://doi.org/10.1021/acs.langmuir.6b01626.
[7] D. Cholakova, N. Denkov, S. Tcholakova, Z. Valkova, S.K. Smoukov, Multilayer formation in self-shaping emulsion droplets, Langmuir 35 (2019) 5484–5495, https://doi.org/10.1021/acs.langmuir.8b02771.
[8] D. Cholakova, D. Glushkova, Z. Valkova, S. Tsibranska-Gyoreva, K. Tsvetkova, S. Tcholakova, N. Denkov, Rotator phases in hexadecane emulsion drops revealed by X-ray synchrotron techniques, J. Colloid Interface Sci. 604 (2021) 260–271, https://doi.org/10.1016/j.jcis.2021.06.122.
[9] E. Sirota, H. King, D. Singer, H. Shao, Rotator phases of normal alkanes: An x-ray scattering study, J. Chem. Phys. 98 (1993) 5809–5824, https://doi.org/10.1063/1.464874.
[10] D. Cholakova, N. Denkov, Rotator phases in alkane systems: in bulk, surface layers and micro/nano-confinements, Adv. Colloid Interface Sci. 269 (2019) 7–42, https://doi.org/10.1016/j.cis.2019.04.001.
[11] S. Guttman, Z. Sapir, M. Schultz, A.V. Butenko, B.M. Ocko, M. Deutsch, E. Sloutskin, How faceted liquid droplets grow tails, Proc. Nat. Acad. Sci. USA 113 (2016) 493–496, https://doi.org/10.1073/pnas.1515614113.
[12] S. Guttman, Z. Sapir, B.M. Ocko, M. Deutsch, E. Sloutskin, Temperature-tuned faceting and shape changes in liquid alkane droplets, Langmuir 33 (2017) 1305–1314, https://doi.org/10.1021/acs.langmuir.6b02926.
[13] O. Marin, M. Tkachev, E. Sloutskin, M. Deutsch, Polyhedral liquid droplets: recent advances in elucidation and application, Curr. Opin. Colloid Interface Sci. 49 (2020) 107–117, https://doi.org/10.1016/j.cocis.2020.05.006.
[14] K. Golemanov, S. Tcholakova, N. Denkov, T. Gurkov, Selection of surfactants for stable paraffin-in-water dispersions, undergoing solid−liquid transition of the dispersed particles, Langmuir 22 (2006) 3560–3569, https://doi.org/10.1021/la053059y.
[15] H. Bunjes, Structural properties of solid lipid based colloidal drug delivery systems, Curr. Opin. Colloid Interface Sci. 16 (2011) 405–411, https://doi.org/10.1016/j.cocis.2011.06.007.
[16] S. He, D. Pascucci, M. Caggioni, S. Lindberg, K. Schultz, Rheological properties of phase transitions in polydisperse and monodisperse colloidal rod systems, AIChE J. 67 (2021) e17401, https://doi.org/10.1002/aic.17401.
[17] A. Chatterjee, L.-M. Wu, Predicting rheology of suspensions of spherical and non-spherical particles using dissipative particle dynamics (DPD): methodology and experimental validation, Mol. Simul. 34 (2008) 243–250, https://doi.org/10.1080/08927020801957748.
[18] M. Khan, R. More, A. Banaei, L. Brandt, A. Ardekani, Rheology of concentrated fiber suspensions with a load-dependent friction coefficient, Phys. Rev. Fluids 8 (2023) 044301, https://doi.org/10.1103/PhysRevFluids.8.044301.
[19] N. Kapate, J. Clegg, S. Mitragotri, Non-spherical micro- and nanoparticles for drug delivery: progress over 15 years, Adv. Drug Deliv. Rev. 177 (2021) 113807, https://doi.org/10.1016/j.addr.2021.05.017.
[20] S. Nejati, E. Vadeghani, S. Khorshidi, A. Karkhaneh, Role of particle shape on efficient and organ-based drug delivery, Eur. Polym. J. 122 (2020) 109353, https://doi.org/10.1016/j.eurpolymj.2019.109353.
[21] T. Moore, A. Cook, E. Bellotti, R. Palomba, P. Manghnani, R. Spanò, S. Brahmachari, M. Di Francesco, A. Palange, D. Di Mascolo, P. Decuzzi, Shape-specific microfabricated particles for biomedical applications: a review, Drug Deliv. Transl. Res. 12 (2022) 2019–2037, https://doi.org/10.1007/s13346-022-01143-4.
[22] R. Toy, P. Peiris, K. Ghaghada, E. Karathanasis, Shaping cancer nanomedicine: the effect of particle shape on the *in vivo* journey of nanoparticles, Nanomedicine 9 (2014) 121–134, https://doi.org/10.2217/nnm.13.191.
[23] K. Yang, Y.Q. Ma, Computer simulation of the translocation of nanoparticles with different shapes across a lipid bilayer, Nat. Nanotechnol. 5 (2010) 579–583, https://doi.org/10.1038/nnano.2010.141.
[24] T. Tree-Udom, J. Seemork, K. Shigyou, T. Hamada, N. Sangphech, T. Palaga, N. Insin, P. Pan-In, S. Wanichwecharungruang, Shape effect on particle-lipid bilayer membrane association, cellular uptake, and cytotoxicity, ACS Appl. Mater. Interfaces 7 (2015) 23993–24000, https://doi.org/10.1021/acsami.5b06781.
[25] S. Himran, A. Suwono, G. Ali Mansoori, Characterization of alkanes and paraffin waxes for application as phase change energy storage medium, Energy Sources 16 (1994) 117–128, https://doi.org/10.1080/00908319408909065.
[26] D. Atinafu, B.Y. Yun, E.E. Kwon, S.J. Chang, S. Kim, Unveiling the effect of molecular chain length on the thermal energy storage capacity and transition temperature of alkane-based phase change composites, Chem. Eng. J. 462 (2023) 142303, https://doi.org/10.1016/j.cej.2023.142303.
[27] H. Peng, D. Zhang, X. Ling, Y. Li, Y. Wang, Q. Yu, X. She, Y. Li, Y. Ding, *n*-alkanes phase change materials and their microencapsulation for thermal energy storage: a critical review, Energy Fuels 32 (2018) 7262–7293, https://doi.org/10.1021/acs.energyfuels.8b01347.
[28] I. Sivebaek, V. Samoilov, B. Persson, Squeezing molecular thin alkane lubrication films between curved solid surfaces with long-range elasticity: layering transitions and wear, J. Chem. Phys. 119 (2003) 2314–2321, https://doi.org/10.1063/1.1582835.
[29] M. Gu, Q. Xia, X. Liu, Y. Guo, Y. Wang, Synthesis of renewable lubricant alkanes from biomass-derived platform chemicals, ChemSusChem 10 (2017) 4102–4108, https://doi.org/10.1002/cssc.201701200.
[30] P. Kamrani, J. Hedrick, J. Marks, A. Zaenglein, Petroleum jelly: a comprehensive review of its history, uses, and safety, J. Am. Acad. Dermatol. (2023), https://doi.org/10.1016/j.jaad.2023.06.010.
[31] E.-K. Park, K.-W. Song, Rheological evaluation of petroleum jelly as a base material in ointment and cream formulations: steady shear flow behavior, Arch. Pharm. Res. 33 (2010) 141–150, https://doi.org/10.1007/s12272-010-2236-4.
[32] J. Reiner, D. Martin, F. Ott, L. Harnisch, V. Gaukel, H. Karbstein, Influence of the triglyceride composition, surfactant concentration and time–temperature conditions on the particle morphology in dispersions, Colloids Interfaces 7 (2023) 22, https://doi.org/10.3390/colloids7010022.
[33] D. Cholakova, S. Tcholakova, N. Denkov, Polymorphic phase transitions in bulk triglyceride mixtures, Cryst. Growth Des. 23 (2023) 2075–2091, https://doi.org/10.1021/acs.cgd.2c01021.
[34] D. Cholakova, Z. Valkova, S. Tcholakova, N. Denkov, B.P. Binks, Spontaneous particle desorption and "Gorgon" drop formation from particle-armored oil drops upon cooling, Soft Matter 16 (2020) 2480–2496, https://doi.org/10.1039/c9sm02354b3.
[35] P. Spicer, R. Hartel, Crystal comets: dewetting during emulsion droplet crystallization, Aust. J. Chem. 58 (2005) 655–659, https://doi.org/10.1071/CH05119.
[36] M. Giso, H. Zhao, P. Spicer, T. Atherton, Crystal comets: a geometric model for sculpting anisotropic particles from emulsions, Langmuir 36 (2020) 13853–13859, https://doi.org/10.1021/acs.langmuir.0c02249.
[37] M. Giso, H. Zhao, P. Spicer, T. Atherton, A phase diagram of morphologies for anisotropic particles sculpted from emulsions, J. Colloid Interface Sci. 605 (2022) 138–145, https://doi.org/10.1016/j.jcis.2021.07.0.
[38] D. Yang, A. Hrymak, Crystal morphology of hydrogenated castor oil in the crystallization of oil-in-water Emulsions: part I. Effect of temperature, Ind. Eng. Chem. Res. 50 (2011) 11585–11593, https://doi.org/10.1021/ie1025985.
[39] N. De Meileir, L. Pellens, W. Broeckx, W. De Malsche, The emulsion crystallization of hydrogenated castor oil into long thin fibers, J. Cryst. Growth 383 (2013) 51–56, https://doi.org/10.1016/j.jcrysgro.2013.08.010.

[40] N. De Meirleir, W. Broeckx, P. Van Puyvelde, W. De Malsche, Surfactant assisted emulsion crystallization of hydrogenated castor oil, Cryst. Growth Des. 15 (2015) 635–641, https://doi.org/10.1021/cg501309m.
[41] S. He, M. Caggioni, S. Lindberg, K. Schultz, Gelation phase diagrams of colloidal rod systems measured over a large composition space, RSC Adv. 12 (2022) 12902–12912, https://doi.org/10.1039/d2ra00609j.
[42] M. Wehrman, S. Lindberg, K. Schultz, Impact of shear on the structure and rheological properties of a hydrogenated castor oil colloidal gel during dynamic phase transitions, J. Rheol. 62 (2018) 437–446, https://doi.org/10.1122/1.4992068.
[43] D. Cholakova, D. Glushkova, S. Tcholakova, N. Denkov, Nanopore and nanoparticle formation with lipids undergoing polymorphic phase transitions, ACS Nano 14 (2020) 8594–8604, https://doi.org/10.1021/acsnano.0c02946.
[44] D. Cholakova, D. Glushkova, M. Pantov, S. Tcholakova, N. Denkov, Triglyceride mixtures: cold-bursting and double emulsion formation, Colloids Surf. A 668 (2023) 131439, https://doi.org/10.1016/j.colsurfa.2023.131439.
[45] S. Arima, S. Ueno, A. Ogawa, K. Sato, Scanning microbeam small-angle X-ray diffraction study of interfacial heterogeneous crystallization of fat crystals in oil-in-water emulsion droplets, Langmuir 25 (2009) 9777–9784, https://doi.org/10.1021/la901115x.
[46] W. Amara-Dali, C. Lopez, P. Lesieur, M. Ollivon, Crystallization properties and polymorphism of triacylglycerols in goat's milk fat globules, Agric. Food Chem. 56 (2008) 4511–4522, https://doi.org/10.1021/jf073491g.
[47] C. Lopez, C. Bourgaux, P. Lesieur, S. Bernadou, G. Keller, M. Ollivon, Thermal and structural behavior of milk fat: 3. Influence of cooling rate and droplet size on cream crystallization, J. Colloid Interface Sci. 254 (2002) 64–78, https://doi.org/10.1006/jcis.2002.8548.
[48] L. Goibier, S. Lecomte, F. Leal-Calderon, C. Faure, The effect of surfactant crystallization on partial coalescence in O/W emulsions, J. Colloid Interface Sci. 500 (2017) 304–314, https://doi.org/10.1016/j.jcis.2017.04.021.
[49] K. Sandra, P. Sandra, G. Vanhoenacker, M. Steenbeke, Profiling nonionic surfactants applied in pharmaceutical formulations by using comprehensive two-dimensional LC with ELSD and MS detection, LCGC North Am. 36 (2018) 385–393. ⟨https://www.chromatographyonline.com/view/profiling-nonionic-surfactants-applied-pharmaceutical-formulations-using-comprehensive-two-dimensi-0⟩.
[50] E. von Meerwall, S. Beckman, J. Jang, W. Mattice, Diffusion of liquid *n*-alkanes: free-volume and density effects, J. Chem. Phys. 108 (1998) 4299–4304, https://doi.org/10.1063/1.475829.
[51] A. Thomas, B. Matthäus, H.-J. Fiebig, Fats and fatty oils. Ullmann's Encyclopedia of Industrial Chemistry, Wiley-VCH, 2015, pp. 1–84, https://doi.org/10.1002/14356007.a10_173.pub2.
[52] T. Gouw, J. Vlugter, Physical properties of triglycerides. I. Density and refractive index, Eur. J. Lipid Sci. Technol. 68 (1966) 544–549, https://doi.org/10.1002/lipi.19660680705.
[53] K. Sato, Crystallization of lipids. Fundamentals and Applications in Food, Cosmetics, and Pharmaceuticals, John Wiley & Sons, 2018.
[54] S. Tcholakova, Z. Valkova, D. Cholakova, Z. Vinarov, I. Lesov, N.D. Denkov, S. K. Smoukov, Efficient self-emulsification via cooling-heating cycles, Nat. Comm. 8 (2017) 15012, https://doi.org/10.1038/ncomms15012.
[55] Z. Valkova, D. Cholakova, S. Tcholakova, N. Denkov, S.K. Smoukov, Mechanisms and control of self-emulsification upon freezing and melting of dispersed alkane drops, Langmuir 33 (2017) 12155–12170, https://doi.org/10.1021/acs.langmuir.7b02048.
[56] D. Cholakova, N. Denkov, Polymorphic phase transitions in triglycerides and their mixtures studied by SAXS/WAXS techniques: in bulk and in emulsions, Adv. Colloid Interface Sci. 323 (2024) 103071, https://doi.org/10.1016/j.cis.2023.103071.
[57] D.M. Small, Lateral chain packing in lipids and membranes, J. Lipid Res. 25 (1984) 1490–1500, https://doi.org/10.1016/S0022-2275(20)34422-9.
[58] K. Larsson, Solid state behavior of glycerides, Ark. Kemi. 23 (1964) 35–56.
[59] K. Sato, T. Kuroda, Kinetics of melt crystallization and transformation of tripalmitin polymorphs, J. Am. Oil Chem. Soc. 64 (1987) 124–127, https://doi.org/10.1007/BF02546266.
[60] I. Norton, C. Lee-Tuffnell, S. Ablett, S. Bociek, A calorimetric, NMR and X-ray diffraction study of the melting behavior of tripalmitin and tristearin and their mixing behavior with triolein, J. Am. Oil Chem. Soc. 62 (1985) 1237–1244, https://doi.org/10.1007/BF02541834.
[61] Z. Weng, P.-Y. Zhang, G.-W. Chu, W. Wang, J. Yun, J.-F. Chen, Performance of alkali-free natural petroleum sulfonates: ultra-low interfacial tension on oil/water interface, Can. J., Chem. Eng. 93 (2015) 1410–1415, https://doi.org/10.1002/cjce.22234.
[62] S. Betancur, L. Giraldo, F. Carrasco-Marín, M. Riazi, E. Manrique, H. Quintero, H. García, C. Franco-Ariza, F. Cortés, Importance of the nanofluid preparation for ultra-low interfacial tension in enhanced oil recovery based on surfactant−nanoparticle−brine system interaction, ACS Omega (14) (2019) 16171–16180, https://doi.org/10.1021/acsomega.9b02372.
[63] H. Princen, I.Y.Z. Zia, S. Mason, Measurement of interfacial tension from the shape of a rotating drop, J. Colloid Interface Sci. 23 (1967) 99–107, https://doi.org/10.1016/0021-9797(67)90090-2.
[64] D. Kashchiev, Nucleation: Basic Theory with Applications, Butterworth Heinemann, Oxford, Boston, 2000, https://doi.org/10.1016/B978-0-7506-4682-6.X5000-8.
[65] R. Sear, Nucleation: theory and applications to protein solutions and colloidal suspensions, J. Phys. Condens. Matter 19 (2007) 033101, https://doi.org/10.1088/0953-8984/19/3/033101.
[66] A. Reynier, P. Dole, S. Humbel, A. Feigenbaum, Diffusion coefficients of additives in polymers. I. Correlation with geometric parameters, J. Appl. Polym. Sci. 82 (2001) 2422–2433, https://doi.org/10.1002/app.2093.
[67] M. Ladd-Parada, M. Povey, J. Vieira, M. Ries, Fast field cycling NMR relaxometry studies of molten and cooled cocoa butter, Mol. Phys. 117 (2019) 1020–1027, https://doi.org/10.1080/00268976.2018.1508784.